Electronic supplementary information (ESI)

Constructing a Triangle Ensemble of Pt Clusters for Enhanced Direct-Pathway Electrocatalysis of Formic Acid Oxidation

Methods

1. Chemicals

Multi-wall carbon nanotubes (MCNTs) were purchased from Timesnano, Chengdu, China (outer diameter (OD), <8 nm; length: 10–30 μm; purity >95%; specific surface area >500 $m^2 g^{-1}$; electric conductivity >100 S cm^{-1}). Potassium permanganate ($KMnO_4$), ethanol (AR, >99.5%), sulfuric acid (95%~98%), ethylene glycol (EG>99.5%) and urea (99%) were purchased from Beijing Tong Guang Fine Chemicals Company. Chloroplatinic acid ($H_2PtCl_6 \cdot 6H_2O$, Pt content ≥37.0%) were purchased from Shanghai Chemical Reagent Co. Ltd. Commercial Pt/C (20 wt%) and Commercial Pt/C (60 wt%) was purchased from Shanghai Hesen Electrical Co., Ltd. All reagents were used as received without further purification. And ultrapure water (resistance: 18.2 MΩ cm) was used to prepare all aqueous solutions.

2. Pretreatment of CNTs

To functionalize the surface of multi-walled carbon nanotubes (CNTs) with oxygen-containing groups, an initial dispersion of 1 g of CNTs was prepared in 60 mL of sulfuric acid. Following this, a measured quantity of 2.5 g of $KMnO_4$ was carefully introduced into the mixture. The ensuing concoction was then subjected to constant agitation at a temperature of 60 °C for a duration of 4 hours. Post-reaction, the system was allowed to return to ambient conditions naturally. Subsequently, it was subjected to centrifugation and thoroughly rinsed with ultra-pure water until neutral. The residual precipitate was then left to dry in an environment maintained at 60 °C overnight.

3. Synthesis of C_3N_4

A quantity of 15 g urea was placed in a crucible and subjected to a temperature of 550 °C in a muffle furnace. This heat treatment was carried out for a period of 4 hours, utilizing a steady heating rate of 5 °C per minute. Following the heating process, the crucible was allowed to cool naturally to ambient temperature. The resultant material was then harvested and reserved for subsequent utilization.

4. Synthesis of Pt-C_3N_4@CNT

50 mg C_3N_4 and 20 mg CNT were dispersed in 20 mL EG and stirred for 30 min, then the mixture was ultrasonically treated for 2 h to obtain a uniform mixture. 1 mL $H_2PtCl_6 \cdot 6H_2O$-EG solution with a certain concentration was added dropwise, stirred and gradually heated to 160 ℃ at the same time, and stayed at 160 ℃ for 3 h. A condensing tube was used during the whole process with flowing water as the heat transfer medium to condense the steam. And the product was cooled naturally until the temperature dropped to room temperature. After that, the resulting precipitates was centrifuged and washed for three times with a mixture solution of 1:1 volume ratio of ultra-pure water and ethanol. Then the final products were dried at 60 ℃ overnight.

The concentration of the platinum precursor solution is determined according to the load of the as-prepared samples. The samples with Pt loadings of 1%, 2%, 3% and 4% were denoted as Pt-C_3N_4@CNT 1, Pt-C_3N_4@CNT 2, Pt-C_3N_4@CNT 3 and Pt-C_3N_4@CNT 4, respectively.

5. Synthesis of Pt@CNT

20 mg CNT was dispersed in 20 ml EG and stirred for 30 min. Then, the mixture was ultrasonically treated for 2 h until it was uniform. 1 mL $H_2PtCl_6 \cdot 6H_2O$-EG solution with a

certain concentration was added drop by drop, then the mixture was stirred and gradually heated to 160 ℃ for 3 h. A condensing tube was used during the whole process with flowing water as the heat transfer medium to condense the steam. After that, the resulting precipitates were centrifuged and washed for three times with a mixture solution of 1:1 volume ratio of ultra-pure water and ethanol. Then the final products were dried at 60 ℃ overnight.

6. Characterization of the samples

The microstructure of the samples was studied using transmission electron microscopy (TEM; FEI Tecnai G220), HRTEM (JEOL, JEM-2100, 200 kV) and AC-HAADF-STEM (JEOL, JEM-ARM 300F) with energy-dispersive spectroscopy (EDS, Sigma, USA). Fourier transform-infrared (FTIR) spectra of the samples were obtained by Bruker Tensor 27 spectrometer. X-ray powder diffraction (XRD) patterns were obtained on a Bruker D8 Advance diffractometer with Cu Kα (λ = 0.15406 nm) radiation and scanning angles (2θ) ranging from 10° to 90°. The chemical compositions of the samples were determined by inductively coupled plasma (ICP) spectroscopy (SPS3100, Seiko Instruments). Raman spectra were obtained on a 532 nm Finder Vista Laser micro-Raman Spectroscopy (Zolix, China). The electronic structure and composition information of the samples were investigated via X-ray photoelectron spectroscopy (XPS, ESCALAB 250).

7. Electrochemical measurements

All measurements were performed on a CHI 660E electrochemical workstation. A three-electrode cell was utilized to perform the electrochemical measurements. Pt wire and Ag/AgCl were used as counter and reference electrodes, respectively. To prepare the working electrode, electrocatalyst was dispersed in the mixture of 800 μL ultrapure water, 200 μL 2-propanol and 10 μL Nafion (5.0 wt%). The mixture was treated by 30- min ultrasonication. Then 4.0 μL ink was dripped on a glass carbon (GC) electrode. The CV and LSV measurements were carried out in an Ar-saturated 0.5 M H_2SO_4 solution and Argon-saturated 0.5 M H_2SO_4 + 0.5 M HCOOH solution with a scan rate of 0.05 V s^{-1}. For CO stripping test, the electrodes were placed in the CO-saturated 0.5 M H_2SO_4 solution with the constant potential held at 0.05 V (vs RHE) for 30 min. Then the electrolyte solution was purged with Ar gas for 15 min to purge the CO dissolved in electrolyte. After that, CO stripping voltammetry curves were collected with a scan rate of 0.02V s^{-1}. The CO bubbling experiment was conducted at 0.40 V (vs. RHE) through chronoamperometry in 0.5 M H_2SO_4 + 0.5 M HCOOH solution. During the chronoamperometric measurements, CO was continuously bubbled into the electrolyte for 200 s.

The measurements of ECSA were carried out via CO-stripping method according to the following equation

$$ECSA=\frac{Q_{CO}}{420\times m_{Pt}} \quad \text{(S1)}$$

where Q_{CO} was obtained by integrating the oxidation peak area of CO, m_{Pt} was the Pt mass on the working electrode, and 420 μC cm^{-2} was the charge required for the oxidation of CO monolayer.

The turnover frequency (TOF) can be used to characterize the intrinsic activity of the each active site in the catalytic reaction process. It can be estimated by the following equations：

$$n = \frac{Qco}{2Fm}$$

where the, n, F, m are represented for the number of active sites, the Faraday constant (96485 C mol^{-1}), and the mass of Pt respectively.

$$TOF = \frac{I}{2Fmn}$$

where I is the current (A) during the cyclic voltammetry measurement and the factor 2 is the number of electrons transferred during the oxidation of formic acid to carbon dioxide.

8. MEA Fabrication and Fuel Cell Test:

First, the Nafion 117 (DuPont) membrane was pretreated in 3.0 wt% H_2O_2 at 80 ℃ for 1.0 h, then it was submerged in ultrapure water at 80 ℃ for 1.0 h. After that, it was treated in 8.0 wt% H_2SO_4 solution at 80 ℃ for 1.0 h. After that, it was treated in ultrapure water at 80 ℃ again for 1.0 h. The MEA with a 1 × 1 cm^2 cell area was fabricated by spray method. The catalyst inks were prepared via dispersing the electrocatalyst into mixture of ultrapure water, isopropanol, and Nafion solution (5.0 wt%). Anode and cathode catalyst inks were directly sprayed onto the pretreated Nafion 117 membrane. The catalyst layer coated on pretreated Nafion 117 membrane was transferred to carbon cloth via hot-pressing at 120 ℃ and 5 MPa for 60 s. The cathode consisted of Pt/C (60 wt%, JM). The anode consisted of Pt-C_3N_4@CNT and Pt@CNT, respectively. The electrocatalyst loading was 0.1 mg $_{Pt}$ cm^{-2} in anode and 0.4 mg $_{Pt}$ cm^{-2} in cathode, respectively.

The single cell configuration consists of two graphite plates with flow fields and gold-plated copper plates as end plate in both sides to avoid corrosion. The steady state polarization curves were obtained by an automatic electric load (PLZ 70UA, Japan). High purity O_2 (99.99 %) was used at the flow rate of 200 mL min^{-1} on the cathode side and 3.0 M formic acid was used at the flow rate of 3.0 mL min^{-1} on the anode side. Prior to the measurement of polarization curves, the single cell was activated at a constant current of 0.05 A for 3 h. For the activation, formic acid and oxygen were supplied to anode and cathode, respectively, and the cell temperature was maintained at 80 ℃. After activation, polarization tests were carried out at the same cell condition and the current range was from 0 to 1A. And the data was collected under the current gradient to obtain the polarization and power density curves to determine the electrical performance of the single cell.

9. DFT Methods

We have employed the first principle to perform all Spin-polarization density functional theory (DFT) calculations within the generalized gradient approximation (GGA) using the Perdew-Burke-Ernzerhof (PBE) formulation [44–46]. We have chosen the projected augmented wave (PAW) potentials to describe the ionic cores and take valence electrons into account using a plane wave basis set with a kinetic energy cutoff of 500eV [47,48]. Partial occupancies of the Kohn–Sham orbitals were allowed using the Gaussian smearing method and a width of 0.2 eV. The electronic energy was considered self-consistent when the energy change was smaller than 10^{-5} eV. The vacuum spacing in a direction perpendicular to the plane of the structure is 15 Å. The Brillouin zone integration is performed using 3×3×1 Monkhorst-Pack k-point sampling for a structure. Finally, the adsorption energies (E_{ads}) were calculated as $E_{ads} = E_{ad/sub} - E_{ad} - E_{sub}$, where $E_{ad/sub}$, E_{ad}, and E_{sub} are the total energies of the optimized adsorbate/substrate system, the adsorbate in the structure, and the clean substrate, respectively. The free energy was calculated using the equation:

$$G = E + ZEP - TS \qquad (S2)$$

where G, E, ZPE and TS are the free energy, total energy from DFT calculations, zero-point energy and entropic contributions, respectively.

Figures

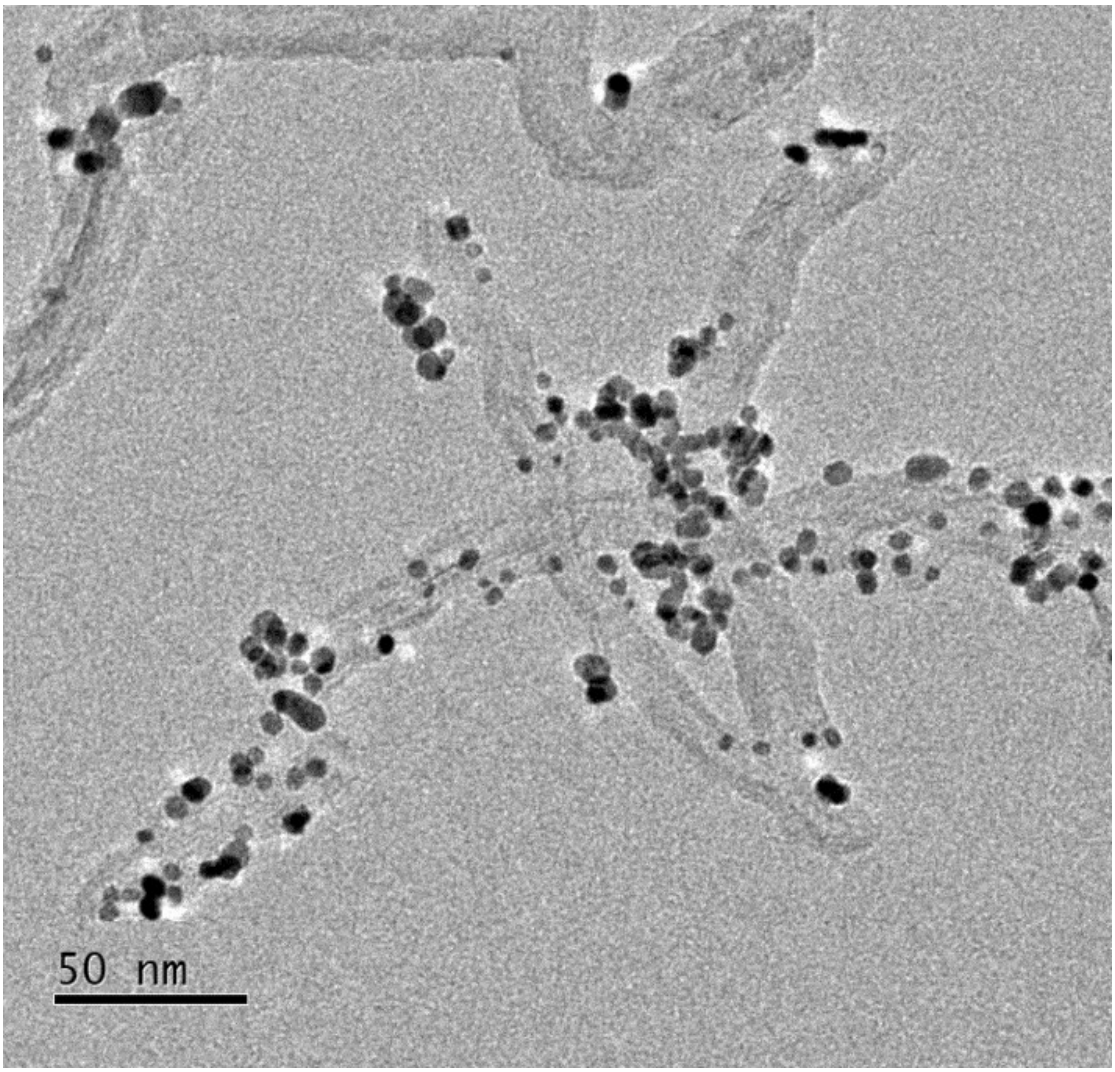

Figure S1. TEM image of Pt@CNT.

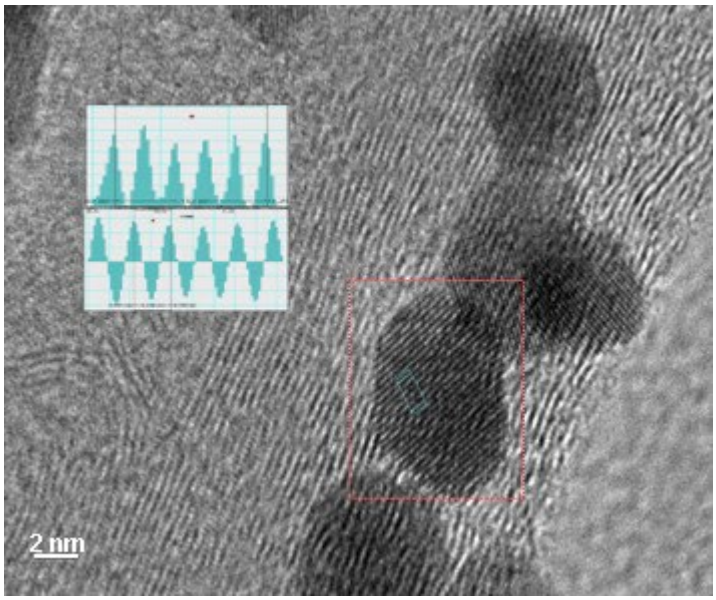

Figure S2. High-resolution TEM image of Pt@CNT.

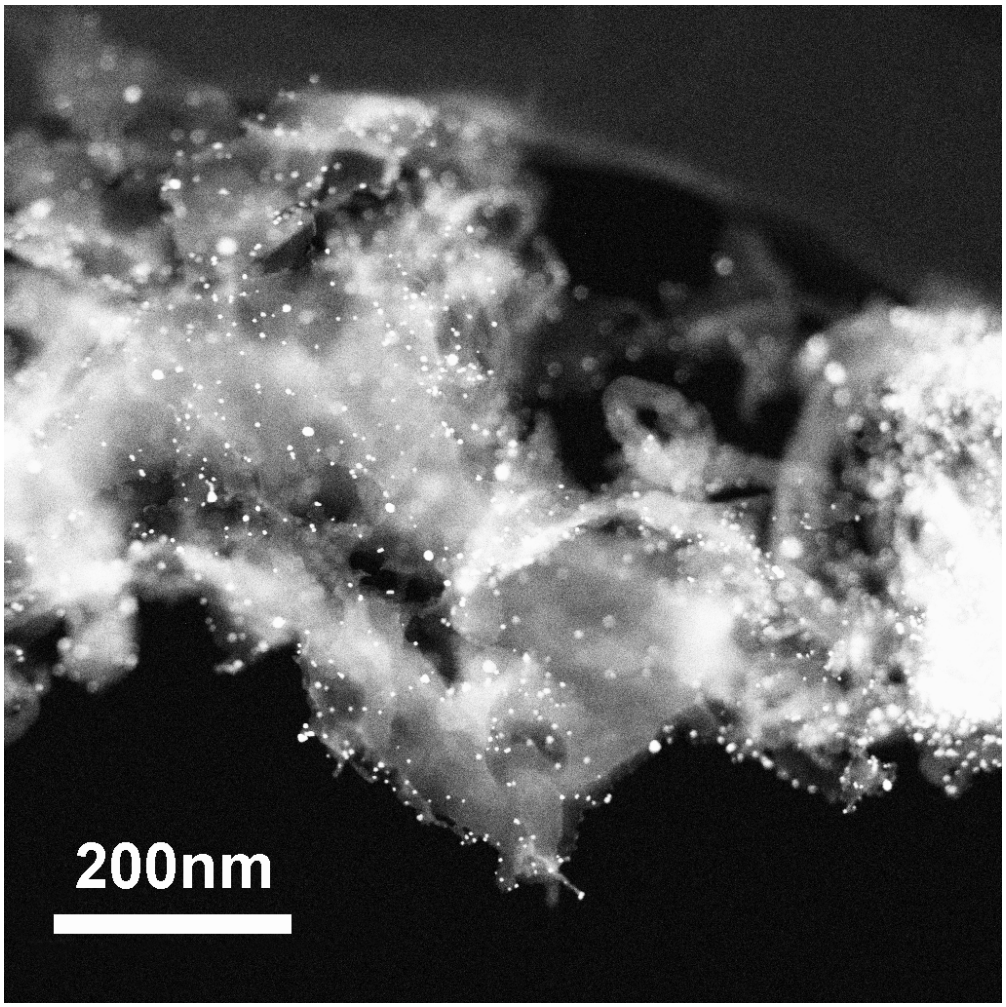

Figure S3. The TEM images of Pt-C_3N_4@CNT after stability tests.

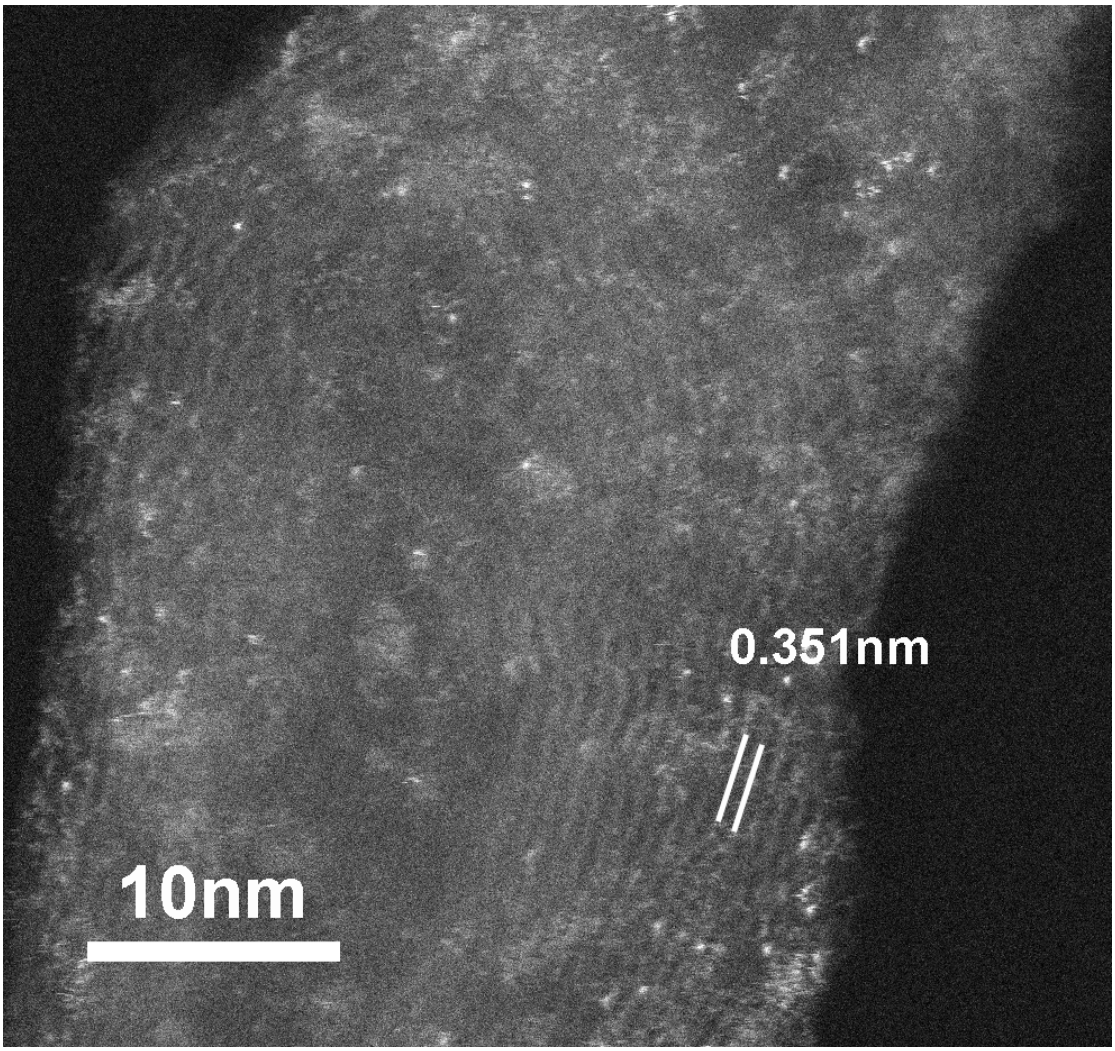

Figure S4. The HRTEM images of Pt-C3N4@CNT after stability tests.

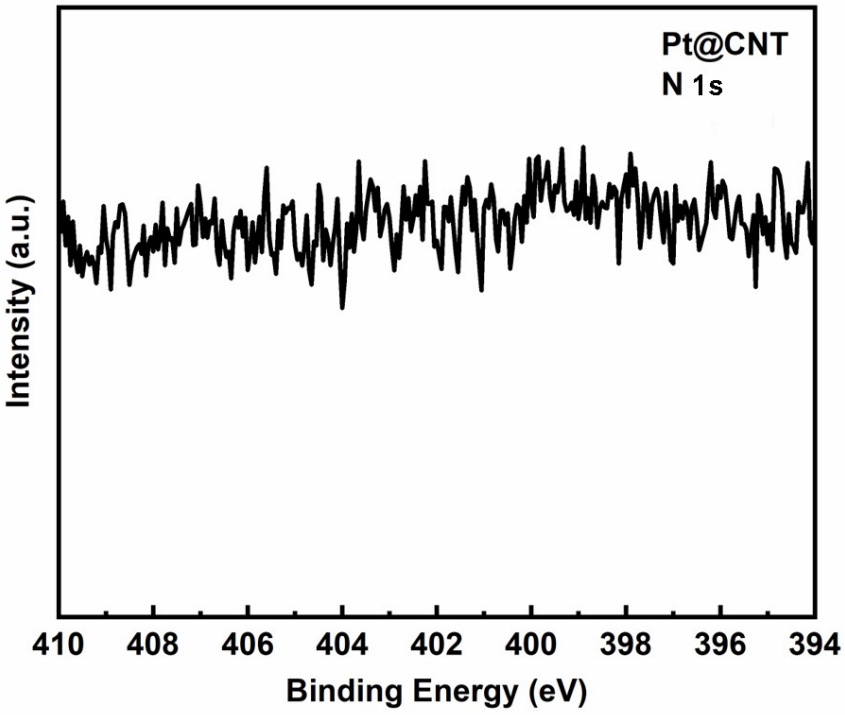

Figure S5. N 1s XPS spectrum of Pt@CNT.

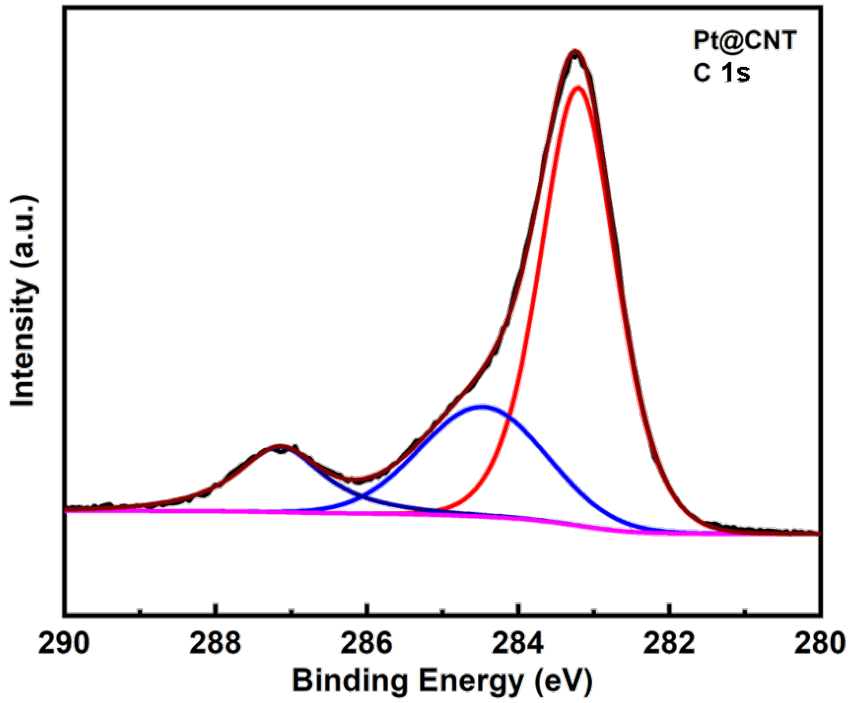

Figure S6. C 1s XPS spectrum of Pt@CNT.

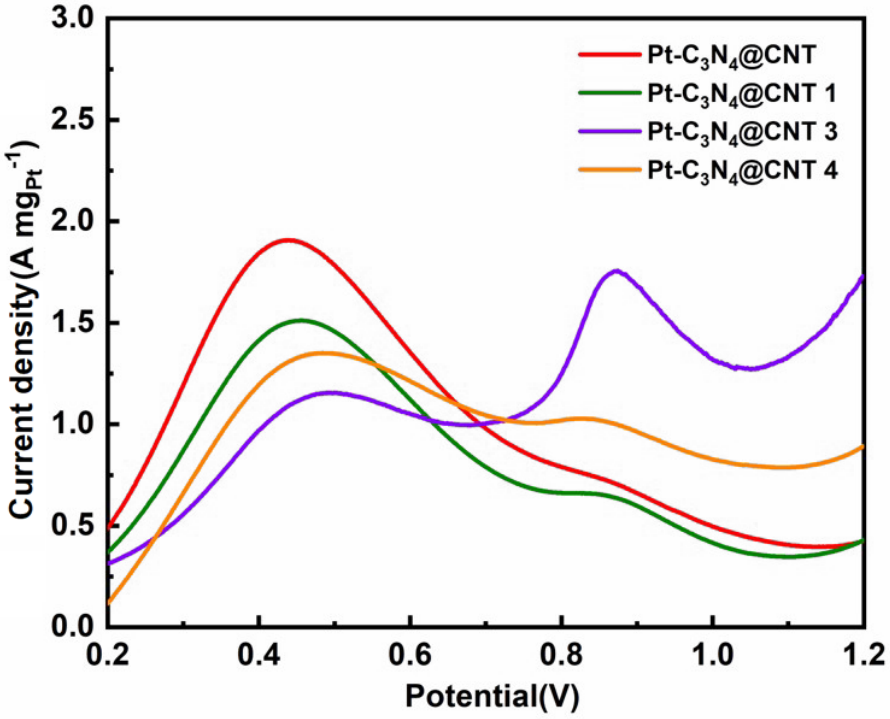

Figure S7. Anodic polarization profiles of Pt-C_3N_4@CNT obtained with different Pt content in 0.5 M H_2SO_4 + 0.5 M HCOOH. Scan rate: 50 mV s^{-1}.

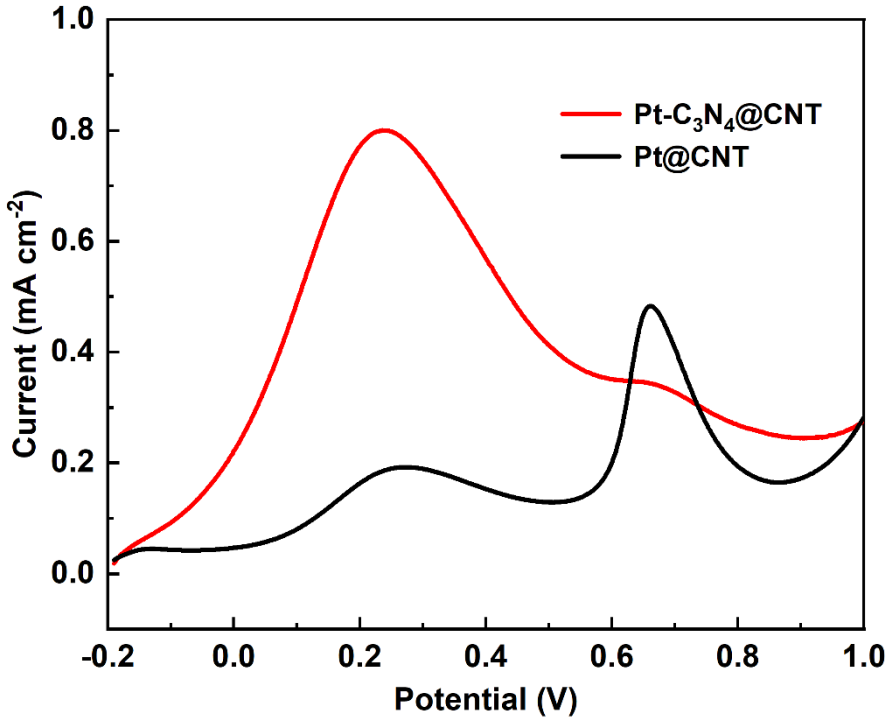

Figure S8. Anodic polarization profiles of Pt-C_3N_4@CNT and Pt@CNT, and shows specific activity of Pt-C_3N_4@CNT and Pt@CNT in 0.5 M H_2SO_4 + 0.5 M HCOOH.

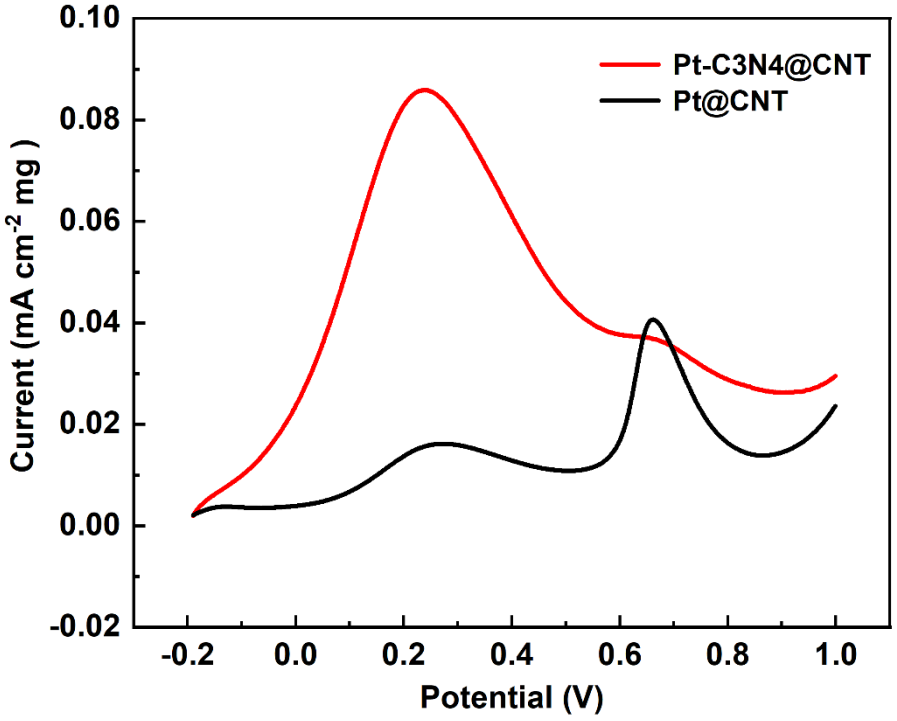

Figure S9. Anodic polarization profiles of Pt-C_3N_4@CNT and Pt@CNT, and shows the current density normalized through ECSA of Pt-C_3N_4@CNT and Pt@CNT in 0.5 M H_2SO_4 + 0.5 M HCOOH.

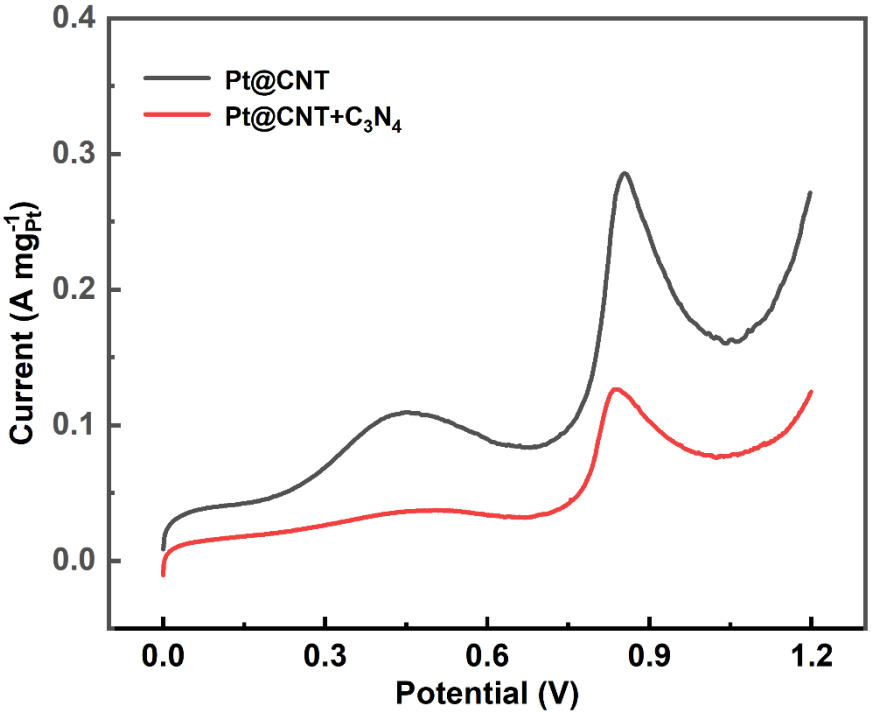

Figure S10. Anodic polarization profiles of the mass activity of Pt@CNT and Pt@CNT mixed with C_3N_4.

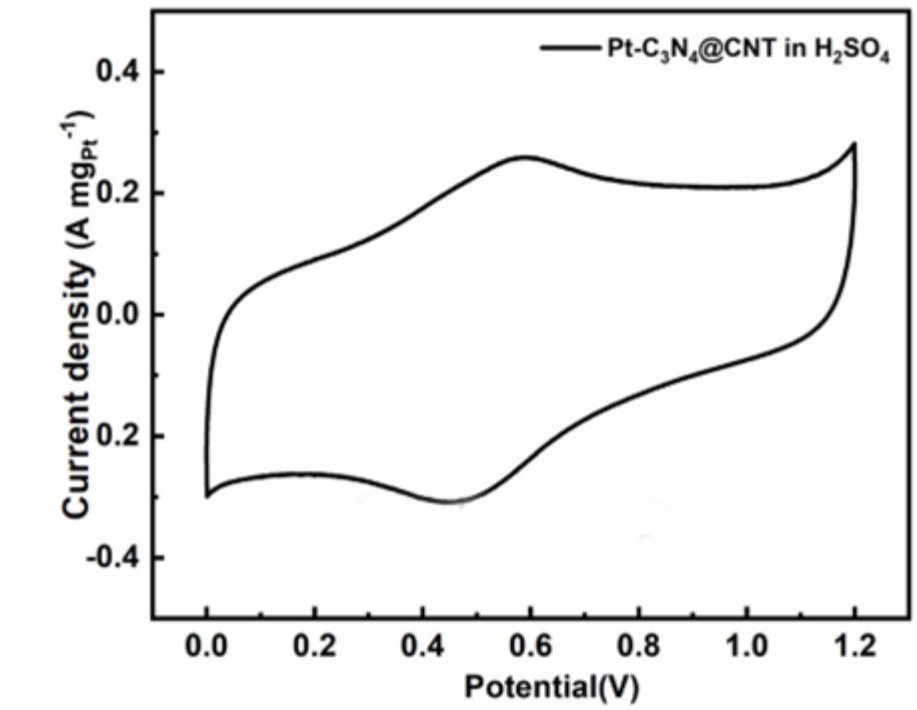

Figure S11. CV curve of Pt-C_3N_4@CNT in 0.5 M H_2SO_4. Scan rate: 50 mV s^{-1}.

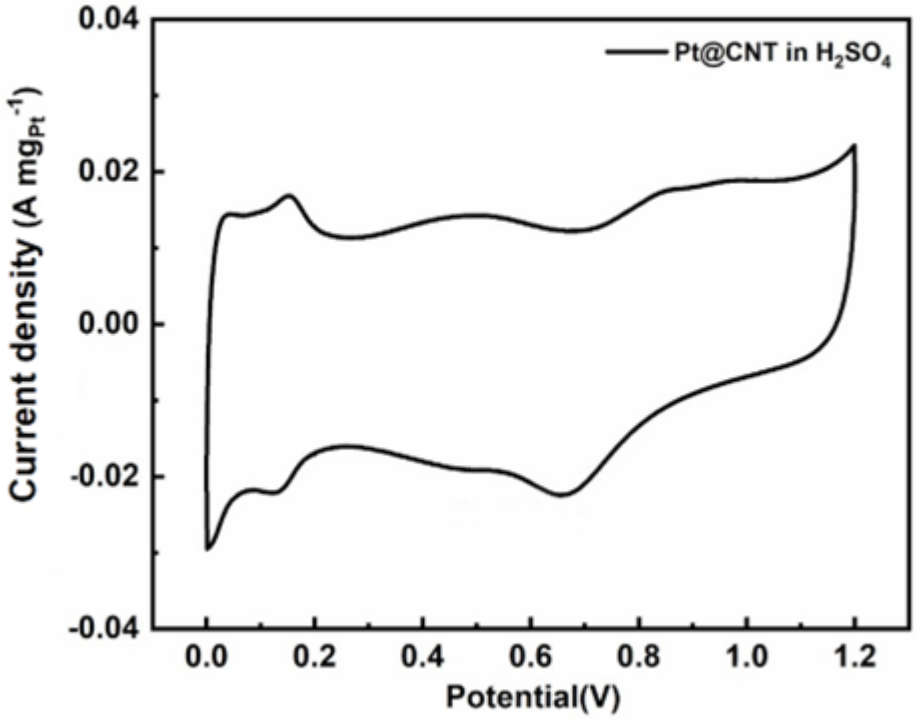

Figure S12. CV curve of Pt@CNT in 0.5 M H_2SO_4 aqueous solution with the scan rate of 50 mV s^{-1}.

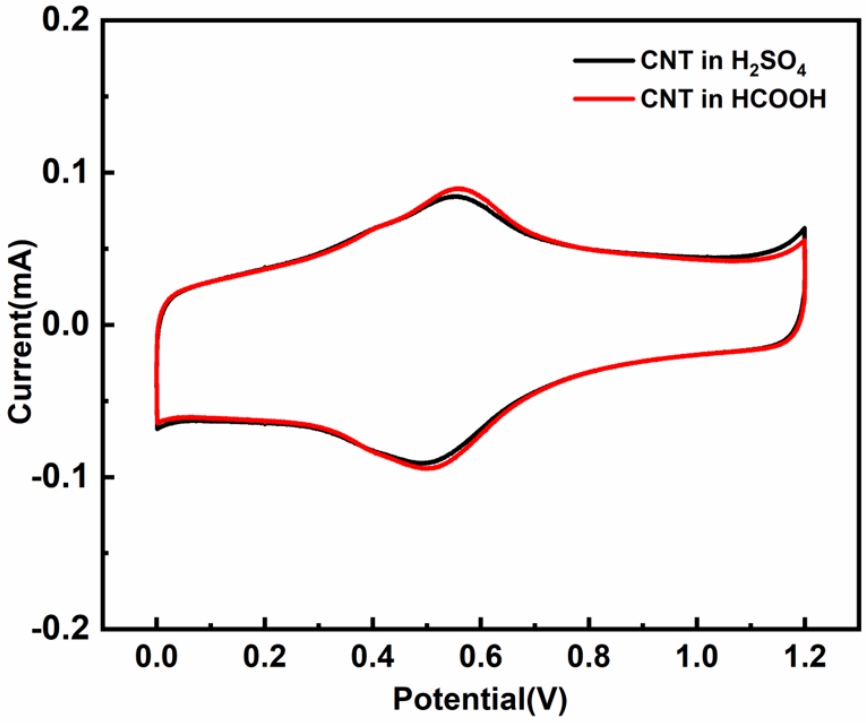

Figure S13. CV curves f of CNT samples in 0.5 M H_2SO_4 aqueous solution (black) , and in 0.5 M H_2SO_4 + 0.5 M HCOOH aqueous solution (red). Scan rate: 50 mV s^{-1}.

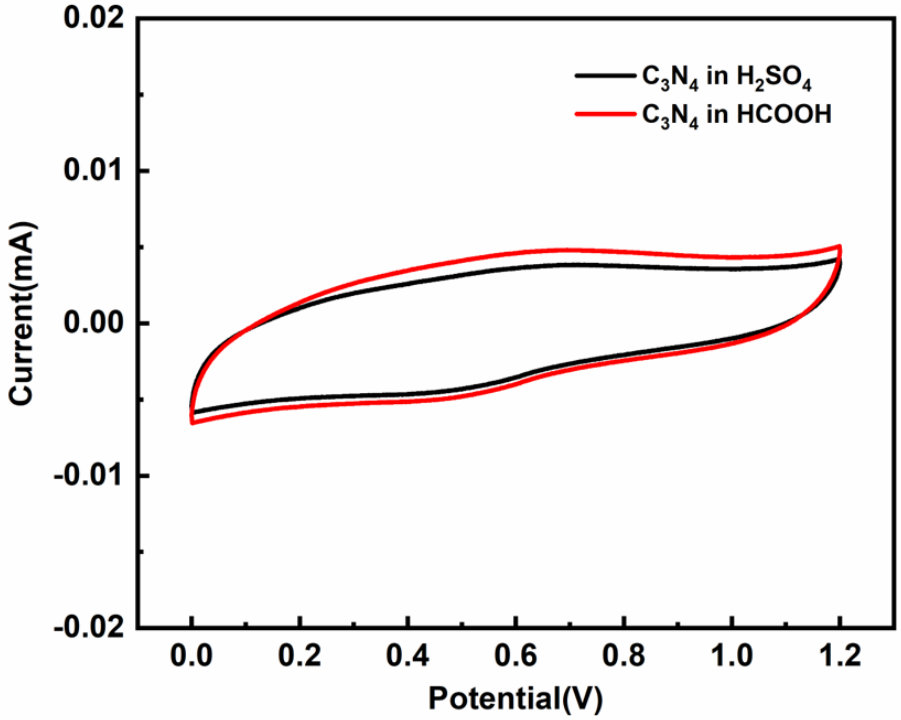

Figure S14. CV curves f of C_3N_4 samples in 0.5 M H_2SO_4 aqueous solution (black), and in 0.5 M H_2SO_4 containing 0.5 M HCOOH aqueous solution (red). Scan rate: 50 mV s^{-1}.

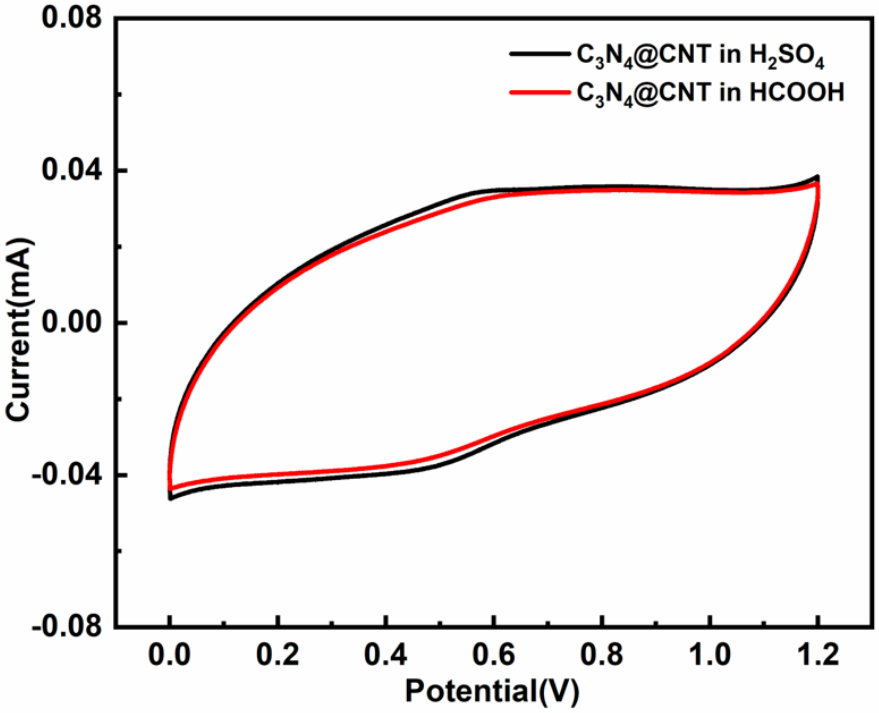

Figure S15. CV curves of C_3N_4@CNT samples in 0.5 M H_2SO_4 aqueous solution (black), and in 0.5 M H_2SO_4 + 0.5 M HCOOH aqueous solution (red). Scan rate: 50 mV s^{-1}.

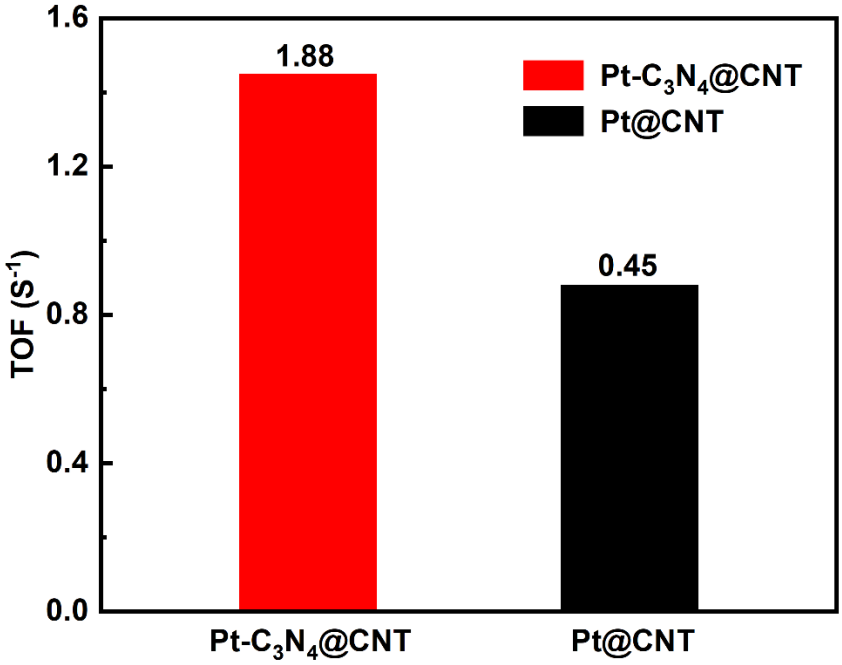

Figure S16. TOF of Pt-C_3N_4@CNT and Pt@CNT.

Table S1. A literature survey of the catalytic activity of Pt-based FAOR catalysts.

Catalysts	Mass activity ($A\ mg^{-1}$)	Specific activity ($mA\ cm^{-2}$)	Refs.
Pt-C3N4@CNT	1.91	0.79	This work
β-$PtBi_2$	1.1	/	[49]
$Pt_{0.05}$Au NWNs	4.99	5.83	[50]
$Pt_{45}Sn_{25}Bi_{30}$	4.39	/	[51]
PtBi@1.8% Pd HNPs	4.17	/	[52]
$Pt_{85}Bi_{15}$ NPs/C	1.50	5.20	[53]
Pt_3Pb-Pt/C	1.48	/	[54]
PtAu/C	1.18	/	[55]
PtAu/CoNC-3	0.88	/	[56]
Pt NWs	0.66	/	[57]
$PtCu_3$/C	0.45	1.57	[12]
Pt-Bi/Au NPs	0.11	/	[58]

Reference

44. Kresse, G.; Furthmüller, J. Efficiency of ab-initio total energy calculations for metals and semiconductors using a plane-wave basis set. *Comput. Mater. Sci.* **1996**, *6*, 15–50, doi:10.1016/0927-0256(96)00008-0.
45. Kresse, G.; Furthmuller, J. Efficient iterative schemes for ab initio total-energy calculations using a plane-wave basis set. *Phys. Rev. B* **1996**, *54*, 11169–11186, doi:10.1103/physrevb.54.11169.
46. Perdew, J.P.; Burke, K.; Ernzerhof, M. Generalized Gradient Approximation Made Simple. *Phys. Rev. Lett.* **1996**, *77*, 3865–3868, doi:10.1103/PhysRevLett.77.3865.
47. Kresse, G.; Joubert, D. From ultrasoft pseudopotentials to the projector augmented-wave method. *Phys. Rev. B* **1999**, *59*, 1758–1775, doi:10.1103/PhysRevB.59.1758.
48. Blochl, P.E. Projector augmented-wave method. Phys. Rev. B **1994**, *50*, 17953–17979, doi:10.1103/physrevb.50.17953.
49. Fu, X.; Li, H.; Xu, A.; Xia, F.; Zhang, L.; Zhang, J.; Ma, D.; Wu, J.; Yue, Q.; Yang, X.; et al. Phase Engineering of Intermetallic $PtBi_2$ Nanoplates for Formic Acid Electrochemical Oxidation. *Nano Lett.* **2023**, *23*, 5467–5474, doi:10.1021/acs.nanolett.3c00528.
50. Shi, H.; Liao, F.; Zhu, W.; Shao, C.; Shao, M. Effective PtAu Nanowire Network Catalysts with Ultralow Pt Content for Formic Acid Oxidation and Methanol Oxidation. *Int. J. Hydrog. Energy* **2020**, *45*, 16071–16079, doi:https://doi.org/10.1016/j.ijhydene.2020.04.003.
51. Luo, S.; Chen, W.; Cheng, Y.; Song, X.; Wu, Q.; Li, L.; Wu, X.; Wu, T.; Li, M.; Yang, Q.; et al. Trimetallic Synergy in Intermetallic PtSnBi Nanoplates Boosts Formic Acid Oxidation. *Adv. Mater.* **2019**, *31*, 1903683, doi:https://doi.org/10.1002/adma.201903683.
52. Tang, M.; Chen, W.; Luo, S.; Wu, X.; Fan, X.; Liao, Y.; Song, X.; Cheng, Y.; Li, L.; Tan, L.; et al. Trace Pd Modified Intermetallic PtBi Nanoplates towards Efficient Formic Acid Electrocatalysis. *J. Mater. Chem. A* **2021**, *9*, 9602–9608, doi:10.1039/D1TA01123E.
53. Li, X.; Sun, Y.; Shen, C.; Zheng, Z.; Chen, H.; Jiang, Y.; Xie, Z. Heterogeneous fcc-Pt/hcp-PtBi Thick-Edge Nanoplates with Enhanced Activity for Formic Acid Oxidation. *ACS Appl. Energy Mater* **2021**, *4*, 9190–9197, doi:10.1021/acsaem.1c01436.
54. Kang, Y.; Qi, L.; Li, M.; Diaz, R.E.; Su, D.; Adzic, R.R.; Stach, E.; Li, J.; Murray, C.B. Highly Active Pt_3Pb and Core–Shell Pt_3Pb–Pt Electrocatalysts for Formic Acid Oxidation. *ACS Nano* **2012**, *6*, 2818–2825, doi:10.1021/nn3003373.
55. Zhang, S.; Shao, Y.; Yin, G.; Lin, Y. Facile Synthesis of PtAu Alloy Nanoparticles with High Activity for Formic Acid Oxidation. *J. Power Sources* **2010**, *195*, 1103–1106, doi:https://doi.org/10.1016/j.jpowsour.2009.08.054.
56. Liang, M.; Xia, T.; Gao, H.; Zhao, K.; Cao, T.; Deng, M.; Ren, X.; Li, S.; Guo, H.; Wang, R. Modulating Reaction Pathways of Formic Acid Oxidation for Optimized Electrocatalytic Performance of PtAu/CoNC. *Nano Res.* **2022**, *15*, 1221–1229, doi:10.1007/s12274-021-3629-z.
57. Xia, B.Y.; Wu, H.B.; Yan, Y.; Lou, X.W.; Wang, X. Ultrathin and Ultralong Single-Crystal Platinum Nanowire Assemblies with Highly Stable Electrocatalytic Activity. *J. Am. Chem. Soc.* **2013**, *135*, 9480–9485, doi:10.1021/ja402955t.
58. Kim, Y.J.; Lee, H.; Chung, H.-S.; Sohn, Y.; Rhee, C.K. Pt-Bi Co-Deposit Shell on Au Nanoparticle Core: High Performance and Long Durability for Formic Acid Oxidation. *Catalysts* **2021**, *11*, 1049, doi:10.3390/catal11091049.